

## Solidification structures of high niobium containing TiAl alloys

Jingwen Xu, Junpin Lin, Yanli Wang, Zhi Lin, and Guoliang Chen

State Key Laboratory for Advanced Metals and Materials, University of Science and Technology, Beijing 100083, China

(Received 2003-12-23)

**Abstract:** To understand the effect of alloy stoichiometry on the microstructural development and mechanical behavior of  $\gamma$ -TiAl-based materials, it is necessary to have a determination of the phase relationships for the TiAl alloy system near the  $\gamma$  phase field. Cast structures and phases of Ti-(43-47)Al-8Nb-(1-2)Mn (at%) alloys have been studied by using scanning electron microscope and X-ray diffraction. Their solidification path and microstructure development during the solidification were analyzed. The experimental results show that the alloys with different Al contents form different macrostructures and microstructural morphologies. This indicates that the solidification paths are different with different Al contents. The alloy with 43Al forms equiaxed grain structure, and the solidification path is as follows:  $L \rightarrow L+\beta \rightarrow \beta \rightarrow \alpha+\beta \rightarrow \alpha+\beta$  cores  $\rightarrow \alpha_2+\gamma+B2$  cores. Whereas the alloy with 47Al forms columnar grain structure, and the solidification path is as follows:  $L \rightarrow L+\beta \rightarrow \alpha+\beta+L \rightarrow \alpha+\gamma+\beta$  cores  $\rightarrow \alpha_2+\gamma+B2$  cores. The  $\beta$  phase is their primary solid phase and can be retained to ambient temperature. The alloy with 43Al solidifies completely into  $\beta$  phase. The peritectic reactions  $L+P \rightarrow \alpha$  and  $L+\alpha \rightarrow \gamma$  appear when the Al content increases to 47Al.

**Key words:** high niobium titanium aluminides; microstructure; phase transformation;  $\beta$  phase

[This research was sponsored by the State Key Project for Fundamental Research Developing Plan (No.G2000067206-2) and the National Natural Science Foundation of China (No. 50274005).]

### 1 Introduction

TiAl-based alloys have been investigated for advanced high temperature structural applications because of their attractive properties such as low density, good elevated temperature strength, high resistance to oxidation and excellent creep property at high temperature. However, the low room-temperature ductility and low toughness of titanium aluminide alloys limit their applications as structural materials. In recent years, many researches have been focused on these titanium aluminide alloys with the addition of alloying elements such as Mo, Nb, W, C, Cr, V, and Mn, and thermomechanical treatment in order to optimize the properties [1].

To understand the effect of alloy stoichiometry on the microstructural development and mechanical behavior of  $\gamma$ -based materials, it is necessary to have a determination of the phase relationships for the Ti-Al system near the  $\gamma$  phase field. In the currently well-accepted Ti-Al binary system [2], the  $\gamma$ -TiAl phase with  $L1_0$  structure is in equilibrium with hexagonal  $\alpha$  or  $\alpha_2$ -Ti<sub>3</sub>Al phase with  $DO_{19}$  structure above and below the eutectoid reaction temperature, respectively, but should never be in equilibrium with disordered bcc

$\beta$ -phase. Most of the alloys under development contain several elements, and the addition of Nb, Mo, Ta, W, V, Cr and Mn have been reported to enhance the formation of  $\beta$  phase [3-10]. The  $\beta$  phase can be retained at room temperature; the retained B2 phase may be either metastable or in equilibrium depending on the degree of stabilization as a function of the nature and amount of alloying elements. The discussion of the solidification structures characterized in the current investigation is available from the work of McCullough *et al.* for binary Ti-Al alloys [2] in the composition range of interest and ternary Ti-Al-Ta alloys [10], and the work of Singh *et al.* for the analysis of the Ti-Al-Mo system [6]. However, until recently the phase relationships among  $\beta$ ,  $\alpha$  and  $\gamma$  phases in the multi-component alloy systems at elevated temperatures have not been well established. In this paper, we describe the as-cast structures of the alloys with Al content ranging from 43at% to 47at%, Mn 1at% or 2at% and Nb 8at%. Their solidification path and microstructure development during the solidification are analyzed.

### 2 Experimental procedure

The alloys with nominal compositions of

Ti43A18Nb1Mn, Ti45A18Nb2Mn and Ti47A18Nb1Mn (all in at%) were analyzed in this study. They were produced from titanium sponge (99.99% in purity), aluminum ingot (99.99%), and Mn and Nb commercial-purity alloys by non-consumable arc melting under pure argon protection. The alloys were first made into buttons. The buttons were flipped three times and remelted to ensure complete mixing of the constituents. Then they were cast in a copper mould. The ingots are shown in **figure 1**.

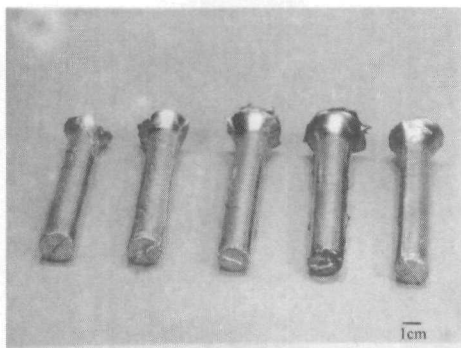


**Figure 1** As-cast ingots of the studied alloys

Metallographic samples were grounded and then electropolished with 7% H<sub>2</sub>SO<sub>4</sub> and 93% methanol at 20°C and ~15 V. The microstructure features were studied by optical microscope and scanning electron microscope (SEM) equipped with an energy dispersive spectrometer (EDS). The SEM was operated in a back-scattered imaging mode to obtain strong atomic number contrast, ideal for imaging segregated structures. Quantitative chemical information was acquired with EDS system calibrated with the appropriate standards.

### 3 Results

Distinct differences are noted in the cast macro-

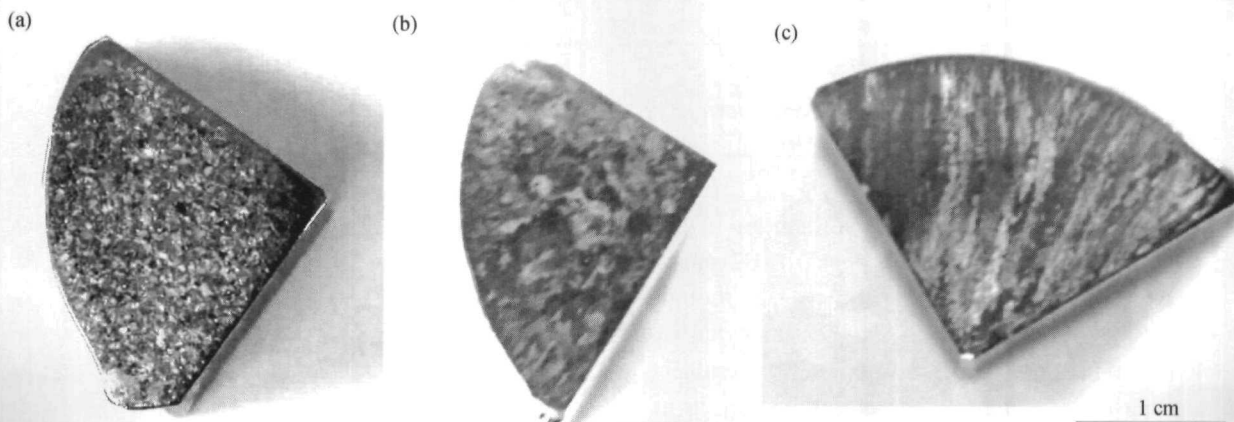


**Figure 2** As-cast macrostructure of Ti43A18Nb1Mn (a), Ti45A18Nb2Mn (b), and Ti47A18Nb1Mn (c) alloys.

The composition of the very bright phase and gray regions around it, as determined by EDS, is given in **table 1**. The bright phase is lean in Al and rich in Nb and Mn and is therefore likely to be B2, the ordered β

structures of the alloys with different Al contents. Grain morphology is equiaxed for Ti43A18Nb1Mn and Ti45A18Nb2Mn alloy. The grain size of Ti43A18Nb1Mn alloy is finer than that of Ti45A18Nb2Mn alloy. Whereas Ti47A18Nb1Mn alloy shows a macrostructure with large columnar grains growing in the cross section. As-cast macrostructures with equiaxed and columnar grains are shown in **figure 2**. This implies that these alloys have different solidification paths.

The backscattered electron (BSE) images of the as-cast Ti43A18Nb1Mn alloy are shown in **figures 3(a)** and **(b)**. The BSE images of the as-cast alloy are composed of large equiaxed grains without dendritic solidification structure. This indicates a complete solidification transformation to (3 phase [2, 11] occurs. The primary transformation product in the solid-state decomposition in 43Al alloy is Widmanstatten plates of a phase with the orientation relationship in a typical "colony" structure, leaving behind thin ribs of retained β. The retained β has bright contrast in the BSE images as shown in figure 3. Several groups of straight, parallel bands of very bright β phase with different directions are presented in most areas, while a network or veined β structure in some of other areas (**figures 3(a), (b)**). During the subsequent cooling, the γ phase precipitates in the α phase in a form of parallel lamellae. The γ lamellae lie on basal planes of the similarly oriented α plates within a colony. The high magnification micrograph (**figure 3 (b)**) shows that the bright β phase is overlapped with the parallel α<sub>2</sub>/γ lamellae of different directions in gray contrast and divides the large α<sub>2</sub>/γ lamellar colonies into fine lamellar colonies by its distribution at sub-grain boundaries.

phase. While the gray α<sub>2</sub>(Ti<sub>3</sub>Al)+γ(TiAl) lamellar regions, signifying the lower average atomic number, contain higher Al but lower Nb and Mn than the former.

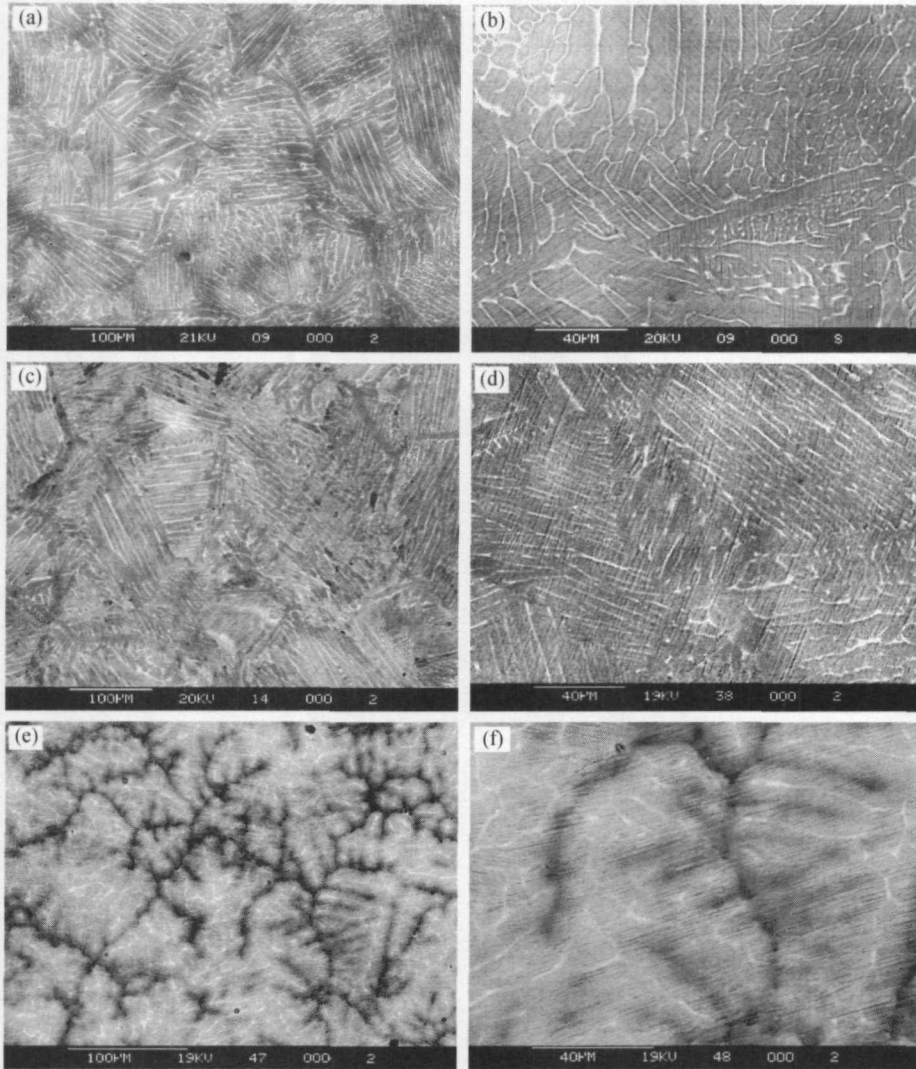


Figure 3 BSE micrographs of the as-cast Ti43A18Nb1Mn (a, b), Ti45A18Nb2Mn (c, d), and Ti47A18Nb1Mn (e, f) alloys.

Table 1 Phase composition in as-cast alloys

Alloy	Phase	Composition / at%			
		Ti	Al	Nb	Mn
Ti43A18Nb1Mn	Primary $\beta$	46.3	39.8	12.4	1.5
	Peritectic $\alpha$	47.3	43.9	7.9	0.7
Ti47A18Nb1Mn	Primary $\beta$	48.1	40.7	9.4	1.8
	Peritectic $\alpha$	44.8	45.8	8.3	1.1
	Interdendritic $\gamma$	42.9	48.3	8.0	0.8

Figure 4 shows the X-ray diffraction pattern of the as-cast Ti43A18Nb1Mn alloy. The peaks of B2 phase are observed in addition to the  $\alpha_2$  and  $\gamma$  peaks though the intensity of B2 (110) peak is lower than that of  $\alpha_2$ (201) and  $\gamma$ (111) peaks in the sample. The result illustrates that the B2 phase coexists with  $\alpha_2$  and  $\gamma$  in the as-cast alloy.

The above features indicate that a complete transformation from liquid to  $\beta$  phase occurs, and a sign of solid-state decomposition paths:  $\beta \rightarrow \alpha$  and  $\alpha \rightarrow \alpha_2 + \gamma$  in the structure exists, but the dendritic solidification structure is not discernible in low magnitude.

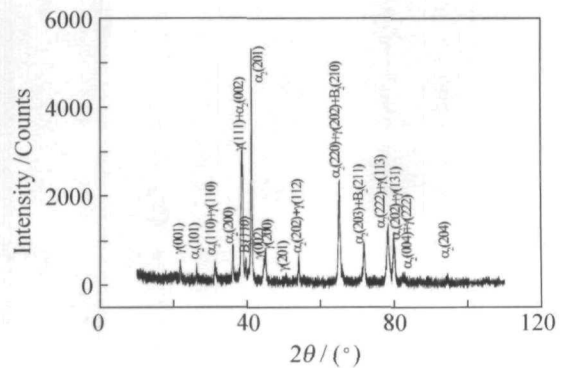


Figure 4 X-ray diffraction pattern of the as-cast Ti43A18Nb1Mn alloy.

Figures 3(c) and (d) are the BES images of the as-cast Ti-45Al-8Nb-2Mn alloy. The as-cast microstructure of this alloy is similar to that of the alloy containing 43Al and 1Mn additions (figures 3(a) and (b)), consisting of large equiaxed grains without dendritic solidification structure. This also indicates a complete transformation to  $\beta$  phase. This shows that they share almost the same transformation paths.

The microstructures of the as-cast Ti-47Al-8Nb-1Mn are shown in figures 3(e) and (f). It is obvious that a dendritic solidification structure exists in the alloys. Such dendritic solidification structure is different from that in the alloys with 43 and 45Al as shown in figure 3. The orthogonal symmetry of a cubic dendrite is evident. And the lamellae traces make an angle of  $45^\circ$  with dendritic arms as shown in figure 3(f). Such a structure is a characteristic of primary solidification into the  $\beta$  phase [2]. The high magnification micrograph (figure 3(f)) shows that a phase in very light contrast, signifying a higher average atomic number, is present within the primary dendrites in the alloy. The primary dendrites cores in very light contrast, which arranged in an orthogonal manner, are surrounded by grayish regions of  $\alpha_2(\text{Ti}_3\text{Al})+\gamma(\text{TiAl})$  lamella and a dark network of the interdendritic  $\gamma$  regions, signifying a lower average atomic number and reminiscent of a peritectic collar [2]. The EDS spectra acquired from the center to the periphery of the dendrites shows that the bright cores are enriched in Ti, Nb and Mn and depleted in Al (table 1), it therefore is proposed to be the retained  $\beta$  phase. Whereas, the dark interdendritic  $\gamma$  regions, where the last liquid solidifies, are enriched in Al, but depleted in the other elements. And the composition of the gray  $\alpha_2+\gamma$  lamella region is between the bright core and dark regions. It is seen that the dendritic structure consists of large lamella colonies, a small amount of segregated  $\gamma$  grains as seen in the base alloy Ti-47Al, and bright B2 cores within lamella colonies. The retained B2 phase is metastable, it can decompose completely after the as-cast alloys are HIPed at  $1200^\circ\text{C}/200\text{ MPa}/4\text{ h}$  [7].

## 4 Discussion

Different cast structures can be obtained at different Al levels, depending on the solidification paths. Ti43Al8Nb1Mn and Ti45Al8Nb2Mn alloys have equiaxed grain macrostructure, and their microstructure shows the evidence of transformation from  $\beta$  to  $\alpha$  phase with different direction plates in figures 3(a) to (d). These are characters of complete solidification of  $\beta$  phase. Whereas, Ti47Al8Nb1Mn alloy shows columnar grain macrostructure, though this is a character of solidification through  $\alpha$ , its primary phase is still  $\beta$  phase because of the orthogonal symmetry of cubic

dendrite arrays, and the  $45^\circ$  lamellae traces with dendritic arms as shown in figures 3(e) and (f).

The geometry of the dendrite arms observed in the microstructure reflects the crystallography of the primary phase. A cubic phase grows from a liquid with dendrite arms in preferential  $\langle 100 \rangle$  directions [12]. It is worth noting here that there are three equivalent directions for  $\langle 100 \rangle$ , namely [100], [010] and [001]. Therefore, the alloys that solidify through the  $\beta$  phase show equiaxed grain rather than columnar character even though the  $\langle 100 \rangle$  axis of the  $\beta$  phase is the preferential direction of crystal growth during solidification. During the solid-state transformation after solidification,  $\beta$  crystals are transformed into  $\alpha$ . Just as in the Ti-Al binary system [2], the orientation relationship between  $\beta$  and  $\alpha$  is  $\{0001\}_\beta // \{110\}_\alpha$ ,  $\langle 11\bar{2}0 \rangle_\beta // \langle 111 \rangle_\alpha$ , inherent in the transformation mechanism involved. Then there are possible twelve orientation variants of  $\alpha$  form during this transformation. The primary equiaxed  $\beta$  grain is gradually consumed by so many groups of different orientation  $\alpha$  plates. Moreover, there is still some  $\beta$  phase retained among these  $\alpha$  plates at room temperature, this is not observed in binary  $\gamma$ -TiAl alloys [2]. The elements Nb and Mn enhance the  $\beta$  stability and retain some of it during cooling. Therefore numerous colonies corresponding to the orientation variants together with some residual B2 phase exist in each of primary  $\beta$  grains. The precipitation of  $\gamma$  within the  $\alpha$  phase occurs subsequently, following the orientation relationship  $(0001)_\alpha // \{110\}_\gamma$  and  $\langle 11\bar{2}0 \rangle_\alpha // \langle 1\bar{1}0 \rangle_\gamma$  in the form of parallel lamellae (figures 3(b) and (d)), which lie on the basal planes of the similarly oriented  $\alpha$  plates within a colony. The as-cast microstructure morphologies of Ti43Al8Nb1Mn and Ti45Al8Nb2Mn alloys in figures 3(a) to (d) indicate the phase transformation mechanisms as discussed above:  $L \rightarrow L+\beta \rightarrow \beta \rightarrow \alpha+\beta \rightarrow \alpha+\beta$  cores  $\rightarrow \alpha_2+\gamma+\text{B2}$  cores. The B2 cores in these alloys are unstable and can decompose during heat-treatment. This will be discussed in further reports.

The dendrites are clearly revealed only in the alloys where enough interdendritic phases segregate to delineate the secondary arms, as shown in the Ti47Al8Nb1Mn alloy, figures 3(e) and (f). Indeed, the retained B2, the  $90^\circ$  angle between dendrite arms and the  $45^\circ$  angle between lamellae traces and dendrite arms observed in the microstructures suggest that the primary  $\beta$  phase forms during the solidification. This conclusion is same as the one reached by Krishnan *et al.* [8]. The retained B2 cores are the natural result of non-equilibrium peritectic solidification. Subsequent peritectic solidification  $L+\beta \rightarrow \alpha$  and finally  $L+\alpha \rightarrow \gamma$  form and cause segregation in ingots cooled through

the  $L+\beta+\alpha$  and  $L+\alpha+\gamma$  fields. The columnar nature, as shown in figure 1(c) and figure 3(f), is due to the preferential crystal growth direction parallel to the  $c$  axis which is unique in the hcp  $\alpha$  phase, which forms during the peritectic solidification.

Solidification velocity is usually too high to approach the equilibrium solidification. Solute redistribution occurs during the solidification of alloys. Micro-segregation can form in the structure of solidified alloys because of limited solute diffusion in liquid and solid during solidification. In our investigation with the addition of  $\beta$ -stabilizing elements Nb and Mn in 47Al alloy, the dendritic segregation formed during solidification is more severe. At the beginning of solidification, the primary  $\beta$  phase forms, in which the content of Nb and Mn is more, and Al is less than the average concentration in the alloy. Al is rejected from the solid-liquid interface and diffuses limitedly into the liquid, so the liquid at the front of the interface of solid-liquid is enriched in Al and depleted in Nb and Mn. As the temperature falls quickly, the composition of the  $\beta$  phase does not homogenize because of the limited diffusion of solutes in the liquid and solid. The dendritic backbone of the ingots is thereby enriched the heavier elements Ti, Nb and Mn. As the solid-liquid interface moves, Al is rejected until the first peritectic reaction causes  $L+\beta \rightarrow \alpha$  transformation. The new  $\alpha$  phase surrounds the primary  $\beta$  phase and the peritectic reaction proceeds only by the diffusion of solutes through the  $\alpha$  phase. The limited diffusion of solutes prevents the peritectic reaction from taking place completely. The primary  $\beta$  at dendrite cores and a small amount of liquid enriched Al at the interdendritic regions still exist till the second peritectic reaction temperature reaches. Then the peritectic reaction  $L+\alpha \rightarrow \gamma$  occurs and forms interdendrite  $\gamma$  phase. During the cooling in solid state, the firstly solidified primary  $\beta$  phase at dendritic cores is retained till ambient temperature and orders into B2, the interdendritic  $\gamma$  grains is also retained. Such dendritic segregation of non-equilibrium microstructures with B2 phase at dendritic cores and  $\gamma$  phase at interdendritic areas is progressively decreased by long term diffusive aging as discussed in reference [7].

## 5 Conclusions

(1) Ti43Al18Nb1Mn and Ti45Al18Nb2Mn alloys form equiaxed grain macrostructures by solidification completely into primary  $\beta$  phase. Whereas peritectic solidification occurs in the alloys with higher Al contents. And peritectic solidification in Ti47Al18Nb1Mn alloy results in a columnar grain structure. Furthermore, Ti47Al18Nb1Mn alloy shows distinct cubic den-

drites with orthogonal symmetry. On the contrary, no such dendrites are observed in Ti43Al18Nb1Mn and Ti45Al18Nb2Mn alloys.  $\beta$  phase is the primary solid phase of all these alloys during solidification and rich in Ti, Nb and Mn. Interdendritic  $\gamma$  forms only in Ti47Al18Nb1Mn alloy containing a higher Al content. These alloys all contain  $\alpha_2$ ,  $\gamma$  and B2 phases.

(2) The phase transformations in Ti-43Al-8Nb-1Mn and Ti-45Al-8Nb-2Mn alloys during cooling are proposed to be  $L \rightarrow L+\beta \rightarrow \beta \rightarrow \alpha+\beta \rightarrow \alpha+\beta$  cores  $\rightarrow \alpha_2+\gamma+B2$  cores. The phase transformations in Ti-47Al-8Nb-1Mn alloy during cooling are proposed to be  $L \rightarrow L+\beta \rightarrow L+\beta+\alpha \rightarrow \alpha+\gamma+\beta$  cores  $\rightarrow \alpha_2+\gamma+B2$  cores.

## References

- [1] Y.W. Kim, Intermetallic alloys based in gamma titanium aluminide, *JOM*, 41(1989), No.7, p.24.
- [2] C. McCullough, J.J. Valencia, C.G. Levi, *et al.*, Phase equilibria and solidification in Ti-Al alloys, *Acta Metall.*, 37(1989), 1321-1336.
- [3] G.L. Chen, W.J. Zhang, Z.C. Liu, and S.J. Li, Microstructure and properties of high-Nb contained TiAl-based alloys, [in] *2nd Int. Sym. on Gamma Titanium Aluminides*, TMS, San Diego, 1999, p.371.
- [4] T.T. Cheng and M.H. Loretto, The decomposition of the beta phase in Ti-44Al-8Nb and Ti-44Al-4Nb-4Zr-0.2Si alloys, *Acta Mater.*, 46(1998), p.4801.
- [5] K. Hashimoto and M. Kimura, Effects of third element additions on mechanical properties of TiAl, [in] R. Darolia, C.T. Liu, P.L. Martin, D.B. Miracle, and M.V. Nathal eds., *Structural Intermetallics*, TMS, 1993, p.309.
- [6] A.K. Singh and D. Banerjee, Transformation in  $\alpha_2+\gamma$  titanium aluminide alloys containing molybdenum: Part I. solidification behavior, *Metall. Mater. Trans.*, 28A(1997), p.1735.
- [7] J.W. Xu, J.P. Lin, Y.L. Wang, and G.L. Chen, Effect of Mn on microstructure of as-cast Ti47Al18Nb(1-2)Mn alloys, *Chin. J. Nonferrous Met.*, 12(2002), No.5, p.818.
- [8] M. Krishnan, B. Natarajan, Vasudevan, *et al.*, Microstructure evolution in gamma titanium aluminides containing beta-phase stabilization and boron additions, [in] *Structure Intermetallics 1997*, The Minerals & Materials Society, Pennsylvania, 1997, p.235.
- [9] Y.R. Zheng, X.H. Yu, S.W. Ma, *et al.*, Effect of Ru on microstructure of cast Ti-47Al alloy, *J. Aeronaut. Mater.* (in Chinese), 19(1999), No.1, p.17.
- [10] J.J. Valencia, C. McCullough, C.G. Levi, *et al.*, Solidification microstructure of supercooled Ti-Al alloys containing intermetallic phases, *Acta Metall.*, 37(1989), p.2517.
- [11] S. NaKa, M. Thomas, C. Sanchez, *et al.*, Development of third generation castable gamma titanium aluminides: role of solidification paths, [in] *Structural Intermetallics 1997*, The Minerals & Materials Society, Pennsylvania, 1997, p.313.
- [12] G.L. Chen and J.P. Lin, *Physical Metallurgy Foundation of Ordered Structural Intermetallics* (in Chinese), Metallurgical Industry Press, Beijing, 1999, p.288.